Journal of Alloys and Compounds 505 (2010) 144–150

Contents lists available at ScienceDirect

Journal of Alloys and Compounds

journal homepage: www.elsevier.com/locate/jallcom

Microstructural and mechanical properties of friction-stir-welded and post-heat-treated Inconel 718 alloy

K.H. Song*, K. Nakata

Joining and Welding Research Institute, Osaka University, 11-1 Mihogaoka, Ibaraki, Osaka 567-0047, Japan

ARTICLE INFO

Article history:
Received 19 April 2010
Received in revised form 25 May 2010
Accepted 1 June 2010
Available online 11 June 2010

Keywords:
High-temperature alloys
Precipitation
Mechanical properties
Transmission electron microscopy (TEM)

ABSTRACT

This study was performed to investigate the microstructural and mechanical properties of friction-stir-welded and post-heat-treated Inconel 718 alloy. Friction stir welding (FSW) was performed at a rotation speed of 200 rpm and welding speed of 150 mm/min; heat treatment was performed after welding at 720 °C for 8 h in vacuum. As a result, the grain size due to FSW was significantly refined from 5 to 20 μm in the base material to 1–3 μm in the stir zone; this was accompanied by dynamic recrystallization, which resulted in enhancements in the mechanical properties as compared to the base material. In particular, applying heat treatment after FSW led to improvements in the mechanical properties of the welds—the microhardness and tensile strength increased by more than 50% and 40%, respectively, as compared to FSW alone.

1. Introduction

Inconel 718, an age hardenable alloy, is widely used in aircraft engines, power plants, and gas turbines due to its good properties such as creep and corrosion resistance and high strengths at high temperatures [1,2]. In general, to manufacture these parts, fusion welding processes such as the application of CO_2 and Nd–YAG lasers and electron beam welding have been employed in recent times [3–5]. However, employing fusion welding processes with the Inconel 718 alloy leads to some problems such as boron/niobium segregation, formation of Laves phase, and liquation cracking in the weld or heat affected zones (HAZs) due to the higher heat input [6,7]. Therefore, in order to solve these problems, it is necessary to make it possible to employ friction stir welding (FSW), which requires lower heat inputs, for welding in the solid state.

Precipitation on Ni-based superalloys plays an important role in improving mechanical properties such as hardness, strength, and creep rupture life [4–6]. In particular, it has been reported previously that the precipitations of gamma double prime (γ'') in the grains and $M_{23}C_6$ carbides in the grain boundaries are effective in improving mechanical properties [4]. However, researches on precipitations with friction-stir-welded Ni-based superalloys have rarely been reported until now [8]. Therefore, in this study, FSW of an age hardenable alloy Inconel 718 was performed in order to investigate the microstructural and mechanical properties of the resulting friction stir welds, and the relationship between precipitation and mechanical properties was evaluated after conducting post-heat treatment.

2. Experimental procedures

The chemical composition of the Inconel 718 alloy used in this study is shown in Table 1. A 150 mm × 32.5 mm × 2 mm sheet of the sample was prepared. FSW was conducted using a WC-Co tool with shoulder diameter of 15 mm, probe diameter of 6 mm, and length of 1.8 mm. Further, in order to obtain sound welds, the tool was tilted at 3° forward from the vertical, and argon gas was utilized to prevent surface oxidation during the welding. FSW was performed at a tool rotation speed of 200 rpm, a tool down-force of 39.2×10^3 N, and a traveling speed of 150 mm/min. After the FSW, in order to investigate the effect of precipitates on the mechanical properties, post-heat treatment was performed at 720 °C (heated up 10 °C/min from room temperature) for 8 h in vacuum of 1×10^{-5} Torr; the samples were then cooled in a furnace from 720 °C to room temperature. A schematic for the post-heat treatment is shown in Fig. 1.

In order to observe macrostructures and microstructures on the welds, a solution comprising 15 ml HCl, 10 ml HNO_3, and 10 ml CH_3COOH was prepared, and samples were etched on the surface after polishing with abrasive paper. Furthermore, in order to evaluate the dispersion of MC carbides in the microstructure, scanning electron microscopy (SEM) and energy dispersive spectroscopy (EDS) analysis were conducted. Also, to evaluate dispersed precipitates such as γ', γ'', and MC carbides in the post-heat-treated specimens, transmission electron microscopy (TEM) analysis was employed. TEM observations were obtained at an acceleration voltage of 200 kV. For the evaluation of mechanical properties, Vickers microhardness tests and tensile tests were conducted. Vickers hardness tests were conducted on the cross-section of the welding zone with a load of 9.8 N and dwell time of 15 s. Two tensile test specimens were used for the tensile tests—to evaluate both the transverse tensile strength of the friction stir welds as well as the longitudinal tensile strength of the stir zone, as shown in Fig. 2.

* Corresponding author. Tel.: +81 6 6879 8668; fax: +81 6 6879 8668.
E-mail address: skhyun7@nate.com (K.H. Song).

0925-8388/$ – see front matter © 2010 Elsevier B.V. All rights reserved.
doi:10.1016/j.jallcom.2010.06.016

Table 1
Chemical composition of Inconel 718 alloy.

Ele.	Ni	Cr	Fe	Mo	Nb	C	Mn	Si	S	Al	Ti
Mass%	52.60	18.60	18.44	3.06	5.30	0.053	0.23	0.06	0.003	0.53	1.01

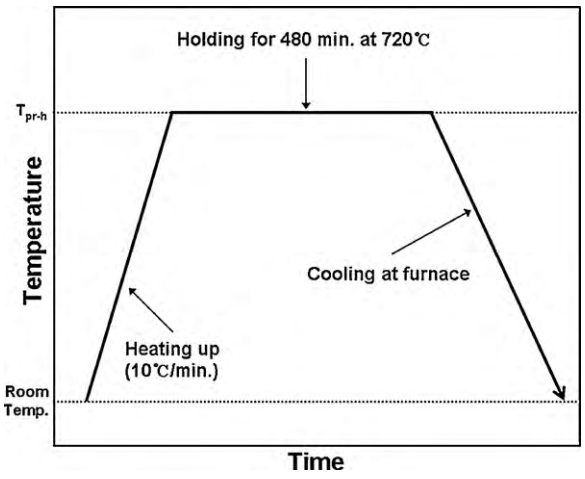

Fig. 1. Schematic of the post-heat treatment cycle. T_{pr-h} indicates the temperature at which precipitation heat treatment was performed.

3. Results

The top view and macrostructure of the friction-stir-welded Inconel 718 alloy are shown in Fig. 3. The specimen was welded at a welding speed of 150 mm/min without causing any defects on the surface, as shown in Fig. 3(a). Furthermore, the specimen was penetrated to 1.7 mm from the top without causing any defects in the weld zone; however, a band structure was observed at the center of the stir zone, as shown in Fig. 3(b). These results are similar to those obtained previously with Inconel 600 and Inconel 625 [8,9]. The temperature hysteresis curve during the FSW is shown in Fig. 4. The temperature was measured on the backside of the plate at the center of the stir zone. The maximum temperature in the stir zone

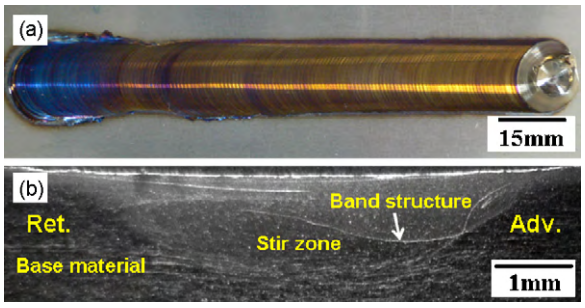

Fig. 3. (a) An external shape and (b) macrostructure of the weld zone. Adv. and Ret. indicate the advancing and retreating sides, respectively.

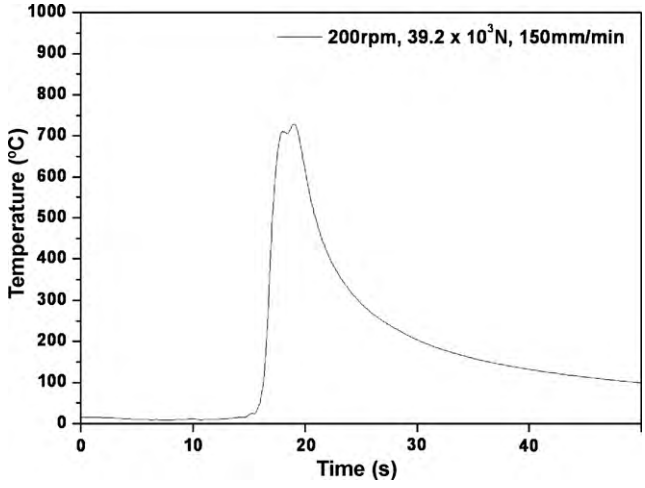

Fig. 4. Temperature hysteresis in the stir zone during the FSW.

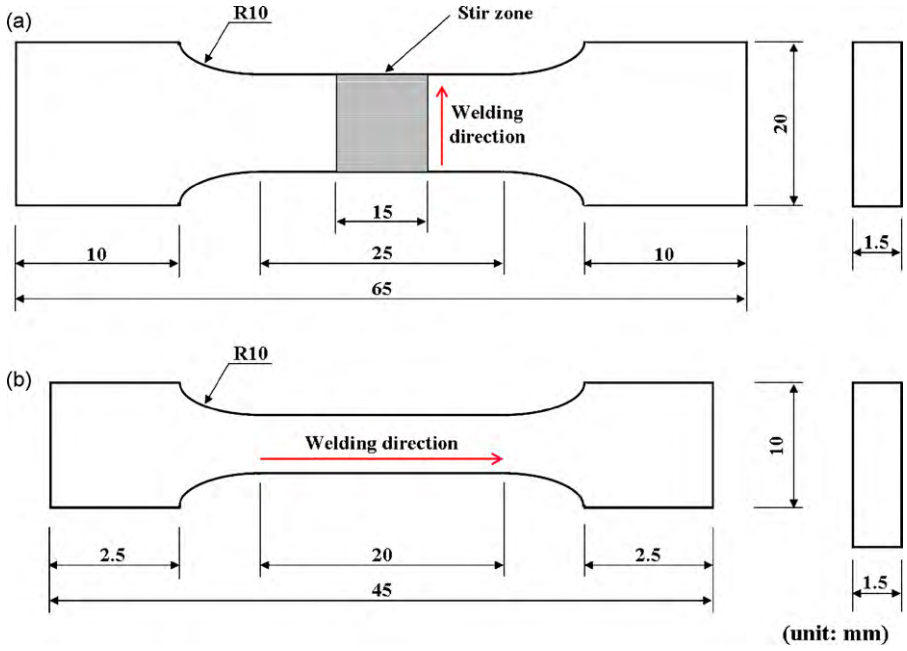

Fig. 2. Configuration of (a) transverse (weld joint) and (b) longitudinal (stir zone) tensile specimens used in this study.

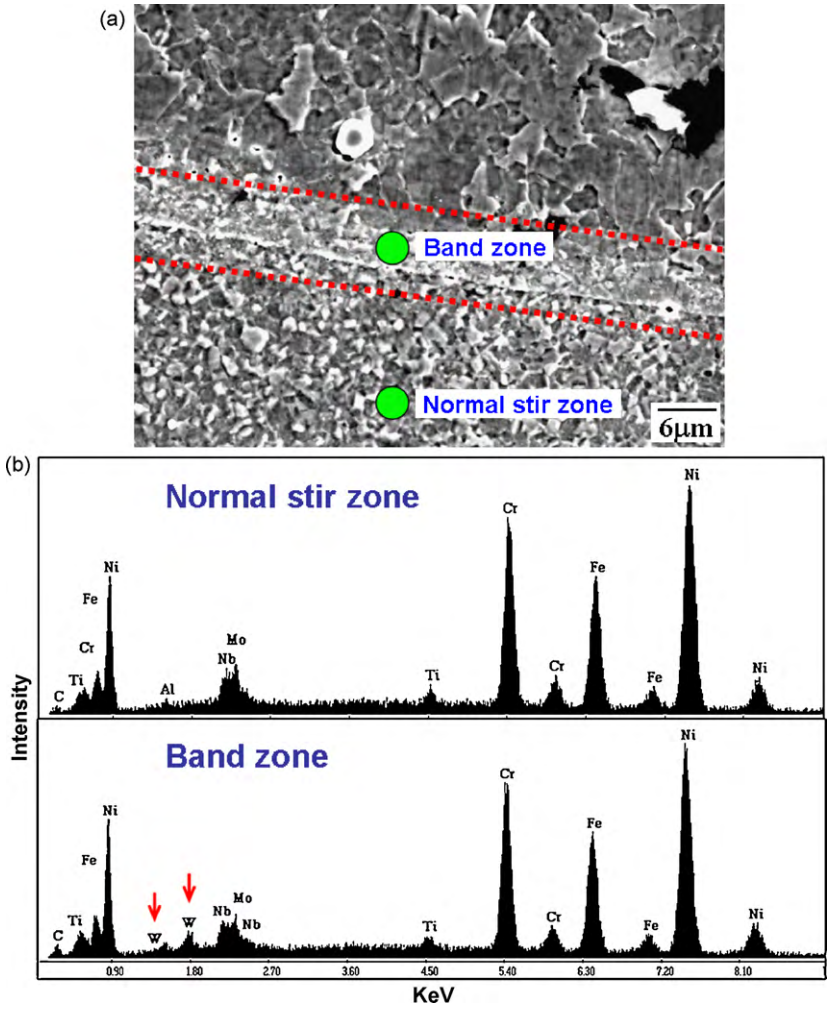

Fig. 5. (a) SEM image and (b) EDS spectrum of the band structure observed at center of the stir zone.

was approximately 740 °C, and it was cooled from 740 to 100 °C in 30 s, as shown in Fig. 4.

The results of the SEM and EDS analyses of the band zone are compared with those for the normal stir zone, as shown in Fig. 5. In Fig. 5(a), the band zone is distributed at the center of the stir zone with a width of 5 μm. From the EDS results, in the band structure, the tungsten element that was primarily dispersed in the tool was detected; however, in the normal stir zone, tool elements such as that in the band zone were not detected, as shown in Fig. 5(b). Similar results were previously obtained in a research conducted on materials with a high melting point [8–10]. Therefore, it is considered that the band structure occurred as a result of tool wear due to the higher friction load between material and tool during FSW.

The microstructures of the friction-stir-welded Inconel 718 alloy are shown in Fig. 6. At the initial state, the base material comprised grains ranging between 5 μm and 20 μm in size; further, annealing twins and MC carbides (arrows in the microstructure) were distributed in the grains and in the grains and grain boundaries, respectively, as shown in Fig. 6(a). On the other hand, the stir zone consisted of more refined grains than those in the base material—their sizes ranged between 1 and 3 μm—as shown in Fig. 6(b). Further, MC carbides similar to those at the base material were observed, but they were more refined. In the case of thermo-mechanically affected zones (TMAZ), deformed grains were observed at the boundary between the base material and stir zone; however, HAZs were not observed in the microstructure due to the absence of grain growth, as shown in Fig. 6(c).

The results of the SEM and EDS analyses of MC carbides observed at the base material and stir zone are shown in Fig. 7. In the base material, MC carbides ranging between 2 and 5 μm in size were dispersed at the grain boundaries and in the grains, as shown in Fig. 7(a); these were estimated to NbC, (Nb, Ti)C and (Nb, Ti, Cr)C, as shown in Fig. 7(c). In the case of the stir zone, the MC carbides were more refined than those of the base material, as shown in Fig. 7(b); however, it also consisted of NbC and (Nb, Ti, Cr)C, as shown in Fig. 7(c).

The TEM image of the stir zone of the post-heat-treated Inconel 718 alloy and the diffraction patterns are shown in Fig. 8. In the stir zone, grains of submicron size were evenly distributed without any dislocation due to the post-heat treatment. Further, intermetallic phase and MC carbides were dispersed in the grains and grain boundaries with its size of 100–200 nm; these were identified as Ni_3Nb (γ''), M_6C, and $M_{23}C_6$ from the diffraction patterns.

The microhardness distribution of the friction-stir-welded and post-heat-treated joint is shown in Fig. 9, as a comparison with that of as-friction-stir-welded joint. The Vickers hardness of the base material was in the range 265–285 Hv, with an average hardness of 273 Hv. In contrast, the microhardness of the stir zone was significantly higher than that of the base material, ranging between 335 and 370 Hv, with an average microhardness of 352 Hv; this is due to the grain refinement in the stir zone. These observations are similar to those for Inconel 600 and 625 alloys [8,9]. A significant increase in the microhardness was observed in all joint positions after the post-heat treatment. As a result, the microhardness in the

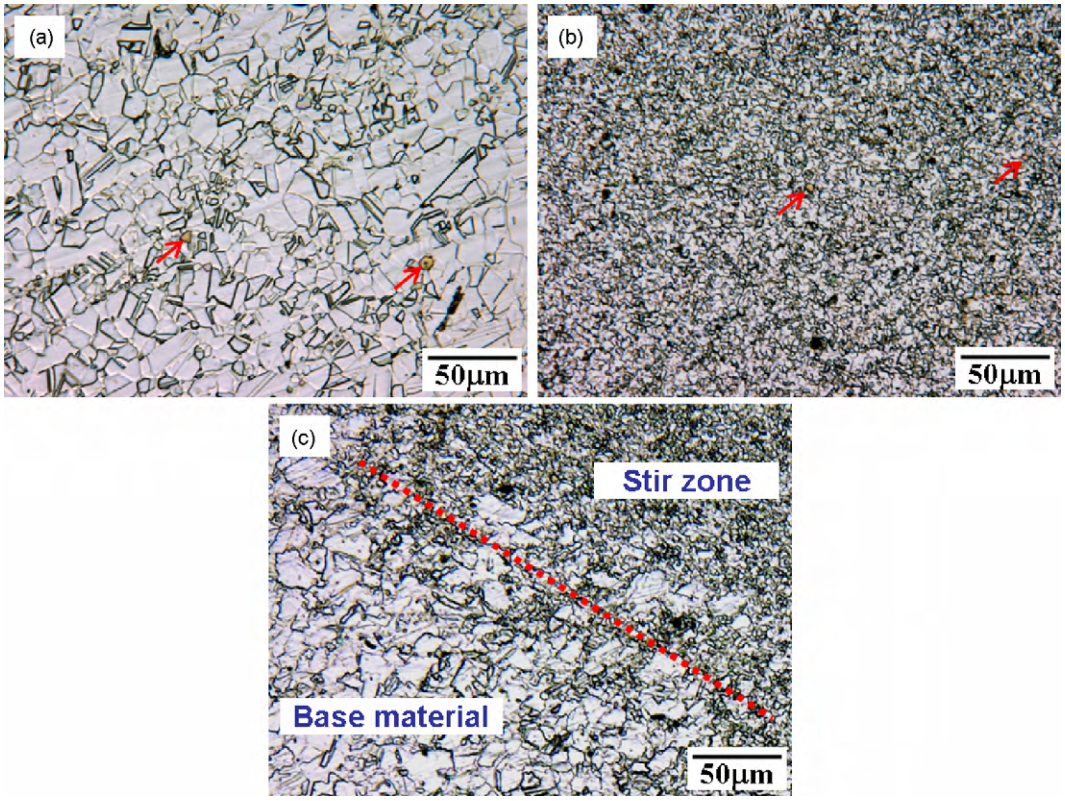

Fig. 6. Microstructures of (a) the base material, (b) stir zone, and (c) thermo-mechanically affected zone (TMAZ) in the friction stir welds.

stir zone reached 525 Hv (490–540 Hv), which is higher than that for the as-friction-stir-welded condition. It is considered that this higher microhardness is due to the combined effect of grain refinement and formation of precipitates by the post-heat treatment in the stir zone.

Top views of the tensile-tested specimens are shown in Fig. 10. The base material was elongated over the entire gage length and fractured at the center of the specimen, as shown in Fig. 10(a). However, the friction-stir-welded joint and post-heat-treated friction-stir-welded joint were preferentially elongated at a part of

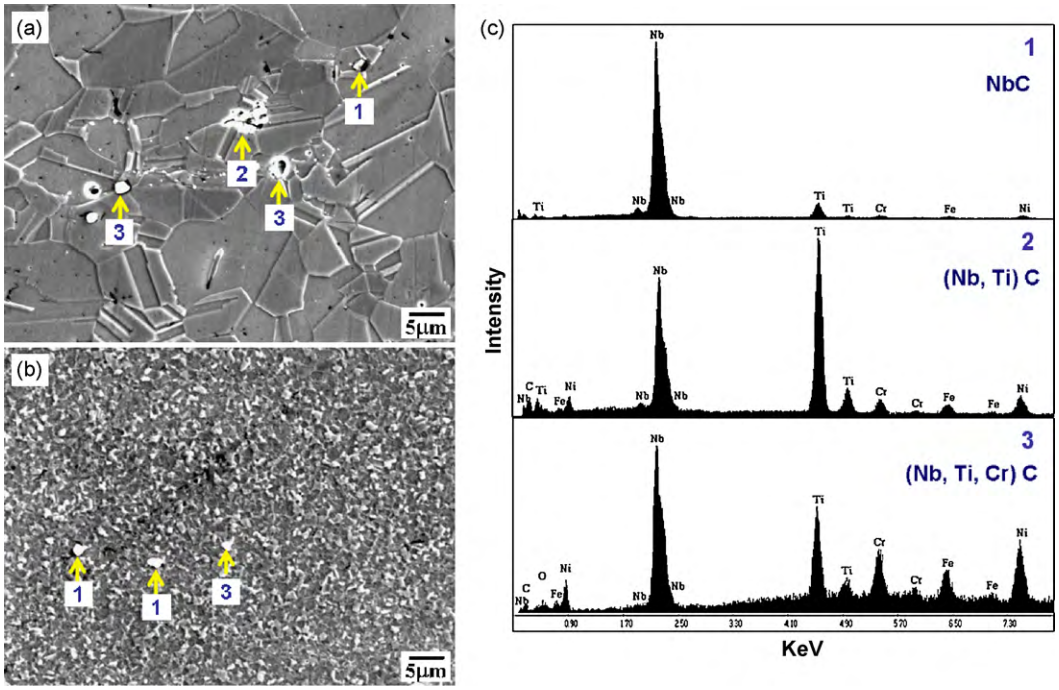

Fig. 7. (a–b) SEM images and (c) EDS spectra of the base material and the stir zone.

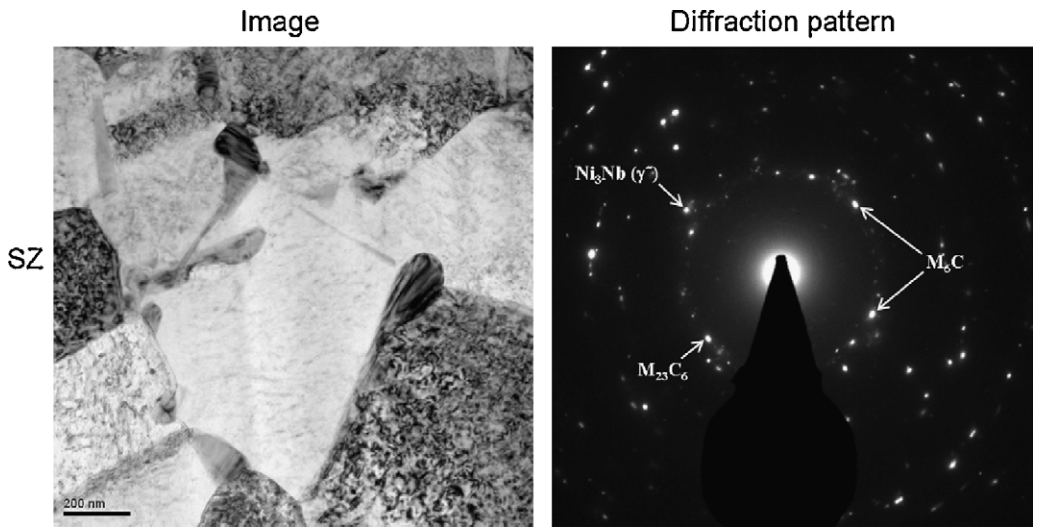

Fig. 8. TEM image and selected area electron diffraction (SAED) pattern of the post-heat-treated Inconel 718 alloy. SZ in this figure indicates stir zone.

the base material and fractured, respectively, due to the effects of the increased strength at the stir zone by the grain refinement and precipitates, respectively, as shown in Fig. 10(b–c). The stir zone specimen was also elongated and fractured at its center, as shown in Fig. 10(d–e).

The tensile properties of the post-heat-treated and as-friction-stir-welded conditions of the friction-stir-welded joint of the Inconel 718 alloy are shown in Fig. 11. Initially, the ultimate tensile strength (UTS) of the base material was 886 MPa in, with an elongation of 52%. The application of FSW led to a slight increase in the UTS, while elongation decreased as compared to the base material; as a result, the UTS on the transverse direction of the welded materials was 961 MPa, and the elongation was 32%. In the case of the stir zone specimens, the UTS was 1135 MPa, which is significantly higher than that of the base material, while the elongation was 28%. In the case of the post-heat-treated friction-stir-welded joint, the UTS was 1426 MPa, i.e., there was a notable significant increase in the strength; however, the elongation decreased to 16%, as compared to the base material. In the case of the post-heat-treated friction-stir-welded stir zone specimen, the UTS was 1570 MPa; this represent a higher strength than that of the heat-treated FSW joint, with an elongation of 15%.

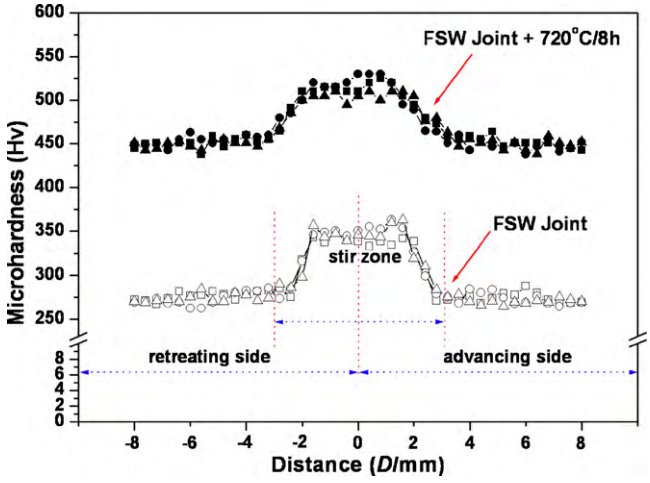

Fig. 9. Distributions of the Vickers microhardness of Inconel 718 FSW joint in comparison with the post-heat-treated and as-friction-stir-welded conditions.

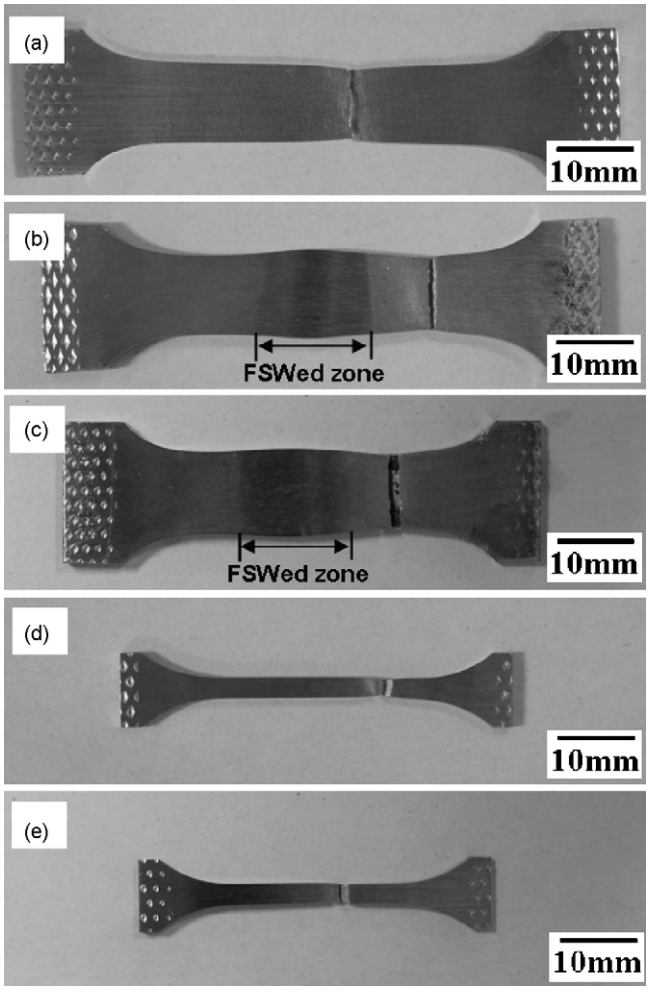

Fig. 10. Top views of specimens subjected to tensile tests. Transverse directions: (a) base material, (b) FSW joint, and (c) post-heat-treated friction-stir-welded joint specimen. Longitudinal direction: (d) friction-stir-welded stir zone and (e) post-heat-treated friction-stir-welded stir zone specimen.

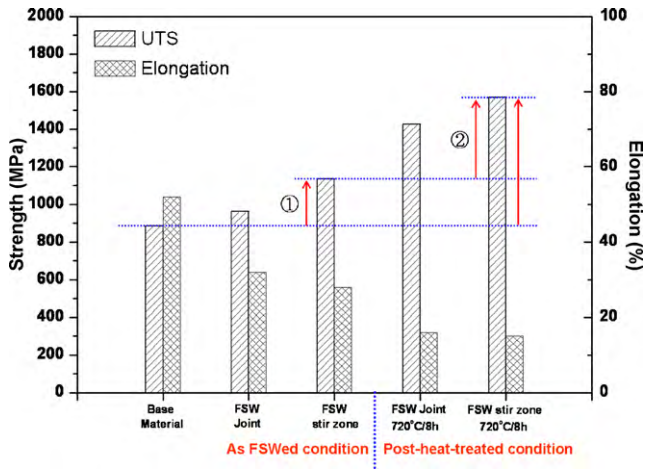

Fig. 11. Tensile properties of the post-heat-treated and as-friction-stir-welded conditions of Inconel 718 alloy. (1) and (2) in figure indicate the increase in strength from that of the base material and the as-friction-stir-welded stir zone, respectively.

4. Discussion

4.1. Grain refinement due to friction stir welding (FSW)

The application of FSW to the Inconel 718 alloy led to grain refinement. As a result, the grains in the stir zone, whose diameters were between 1 and 3 μm, were more significantly refined than those of the base material, whose diameters ranged between 5 and 20 μm, as shown in Fig. 6. The grain refinement can be explained in terms of dynamic recrystallization by severe deformation and heat input during FSW. In other words, during FSW, the strain rates (stored energy) due to the plastic flow in the stir zone are high and friction heat is present between the material and tool [11–13]. Furthermore, in this study, the peak temperature at the center of the stir zone was measured as 740 °C, which is sufficient for recrystallization the Inconel 718 alloy, as shown in Fig. 4. Moreover, the cooling time from peak temperature (740 °C) to a lower temperature (100 °C) was approximately 30 s, which is sufficient for protection from the grain growth after the recrystallization, as shown in Fig. 4. Therefore, along with the high strain rate, sufficient heat input and fast cooling times during FSW easily lead to grain refinement.

The material used in this study, Inconel 718 alloy, has low stacking fault energy of FCC metals [14]. In general, these materials can easily undergo dynamic recrystallization, as compared to materials with high stacking fault energies such as Al alloys; on the other hand, it is difficult to rearrange the dislocation by dynamic recovery [15,16]. In other words, materials with low stacking fault energies can lead to recrystallization nuclei more easily than materials with high stacking fault energies. Furthermore, if the higher dislocation density is accompanied by severe deformation during the FSW, the formation of dense recrystallization nuclei is significantly promoted. Therefore, recrystallization nuclei can be simultaneously created at the grains and grain boundaries having higher densities at dislocations. In this manner, it can be stated that grain refinement can be obtained by the FSW.

4.2. Enhancement in mechanical properties due to FSW

Mechanical properties such as microhardness and tensile strength were enhanced by FSW. This can be explained on the basis that after FSW, the grain sizes in the stir zone are smaller than those in the base material. In the case of microhardness, the base material microhardness ranged between 265 and 285 Hv, whereas, in the stir zone, the microhardness ranged from 335 to 370 Hv; this represents an increase of more than 30% when compared to the base material, as shown in Fig. 9. These increases in the microhardness were caused by the grain refinement in the stir zone, where grain sizes ranged between 1 and 3 μm in diameter, as compared to the base material grain sizes ranging between 5 and 20 μm, as shown in Fig. 6. In general, the grain size influenced mechanical properties such as hardness and strength; in this manner, the effect of the grain refinement is clearly indicated in this study.

The results of the tensile tests also accurately showed the increase in strength due to the grain refinement. In transverse tensile tests of the joint, the base material was first deformed and fractured due to its coarsened grain size as compared to case of the stir zone joint (see Fig. 10). In the case of longitudinal tensile-tested specimens in the stir zone, the strength significantly increased to 25% more than that of the base material. As a result, the UTS increased from 886 MPa in the base material to 1135 MPa in the stir zone, as shown in Fig. 11. In this manner, these results also clearly show the effect of the grain refinement.

4.3. Effect of precipitates due to post-heat treatment

The Inconel 718 alloy is strengthened by the formation of precipitates such as MC carbides and intermetallic phases at elevated temperatures [17,18]. These precipitates play an important role in enhancing mechanical properties such as hardness, strength, and creep rupture life [4–6]. As the experimental result, the post-heat treatment after FSW led to the formation of precipitates in the specimen. In particular, in the post-heat-treated stir zone, precipitates such as Ni_3Nb (γ''), M_6C, and $M_{23}C_6$ were observed in the grains and at the grain boundaries, similar to those at the Inconel 625 alloy [8], as shown in Fig. 8. Furthermore, these precipitates were dispersed at the grain boundaries and in the grains; with a size of 100–200 nm, they had a significantly fine structure.

In the post-heat-treated Inconel 718 alloy as well, an enhancement in mechanical properties such as microhardness and tensile strength was observed due to precipitates, despite the slight grain growth by the post-heat treatment. At the FSW joint, the microhardness of the base material and stir zone was 273 and 352 Hv on an average, respectively, as shown in Fig. 9. In contrast, in the post-heat-treated friction-stir-welded joint, the microhardness of the base material and stir zone was greater than that of the friction-stir-welded joint, as shown in Fig. 9—370 Hv (base material) and 435 Hv (stir zone). The friction-stir-welded and post-heat-treated friction-stir-welded joints exhibited tensile strengths of 961 and 1426 MPa, respectively, as shown in Fig. 11. Therefore, in this manner, the effect of precipitation strengthening due to the post-heat treatment has been accurately shown.

5. Conclusions

FSW was successfully performed on the Inconel 718 alloy at a welding speed of 150 mm/min in without leading to any defects in the welds. As a result, the application of FSW led to grain refinement from 10 μm, on an average, in the base material to 1–3 μm in the stir zone, and it was accompanied by dynamic recrystallization. This grain refinement was effective in enhancing and improving mechanical properties—microhardness significantly increased from 273 Hv in the base material to 352 Hv in the stir zone. The tensile strength also increased from 886 MPa in the base material to 1135 MPa in the stir zone, which implies fracture in the base material at the joint. Furthermore, the mechanical properties were enhanced by post-heat treatment due to the formation of precipitates such as MC carbides and intermetallic phase at elevated temperatures. As a result, the post-heat-treated specimen showed

significantly increased for microhardness distribution than the FSW joint at approximately 40%; the tensile strength was also more than 30%. Such enhancements in the mechanical properties were caused by the formation of precipitates during the post-heat treatment. Therefore, in this manner, Inconel 718 alloy can exhibit enhanced mechanical properties if post-heat treatment is performed after FSW.

Acknowledgements

The authors thank Prof. H. Fujii and Mr. Y.D. Jung for performing the heat treatment of the materials.

References

[1] E.A. Loria, J. Met. 40 (1988) 36–41.
[2] T.S. Chester, S.S. Norman, C.H. William, Superalloys, Wiley, 1987.
[3] J.K. Hong, J.H. Park, N.K. Park, I.S. Eom, M.B. Kim, C.Y. Kang, J. Mater. Proc. Tech. 201 (2008) 515–520.
[4] S. Gobbi, L. Zhang, J. Norris, K.H. Richter, J.H. Loreau, J. Mater. Proc. Tech. 56 (1996) 333–345.
[5] C.A. Huang, T.H. Wang, C.H. Lee, W.C. Han, Mater. Sci. Eng. A 398 (2005) 275–281.
[6] W. Chen, M.C. Chaturvedi, N.L. Richards, Metall. Trans. A 32 (2001) 931–939.
[7] T.J. Kelly, Weld. J. 68 (1989) 44–51.
[8] K.H. Song, K. Nakata, Mater. Des. 31 (2010) 2942–2947.
[9] K.H. Song, H. Fujii, K. Nakata, Mater. Des. 30 (2009) 3972–3978.
[10] K.H. Song, T. Tsumura, K. Nakata, Mater. Trans. 50 (2009) 1832–1837.
[11] R.S. Mishra, M.W. Mahoney, Friction Stir Welding and Processing, ASM Int, 2007.
[12] Z. Zhang, H.W. Zhang, J. Mater. Proc. Tech. 209 (2009) 241–270.
[13] H.W. Zhang, Z. Zhang, J.T. Chen, J. Mater. Proc. Tech. 183 (2007) 62–70.
[14] J.M. Howe, Interfaces in Materials, Wiley-Interscience, 1997.
[15] F.J. Humphreys, M. Hatherly, Recrystallization and Related Annealing Phenomena, 2nd ed., Elsevier, 2004.
[16] R.E. Reed-Hill, R. Abbaschian, Physical Metallurgy Principles, 3rd ed., 1991.
[17] G. Appa Rao, M. Kumar, M. Srinivas, D.S. Sarma, Mater. Sci. Eng. A 355 (2003) 114–125.
[18] J. He, G. Han, S. Fukuyama, K. Yokogawa, Acta Mater. 46 (1998) 215–223.